GEOPHYSICS, VOL. 81, NO. 3 (MAY-JUNE 2016); P. T117–T129, 15 FIGS., 2 TABLES.
10.1190/GEO2014-0522.1

Separating a wavefield by propagation direction

Alan Richardson[1] and Alison E. Malcolm[2]

ABSTRACT

Determining the propagation direction of waves in a wavefield is important in several seismic imaging techniques and applications, including velocity analysis, amplitude variation with angle analysis, survey design, and illumination compensation. This can be achieved using the Poynting vector method, but this method performs poorly when waves overlap, returning incorrect wave amplitude and direction. An alternative, the local slowness method, is capable of separating overlapping waves, but it suffers from low angular resolution. We have developed modifications of these two approaches that improve the ability to extract the wave amplitude propagating in different directions. The primary modification is the addition of a wavefront orientation separation step. We have evaluated the methods' ability to separate six overlapping waves with different phases in a constant velocity model, to accurately determine scattering angles in the construction of an angle domain image gather, and to determine the propagation directions of the back-propagated receiver wavefield for one shot in a 2D slice of the SEAM model. We have determined that in these examples, the proposed methods produce results that are generally superior to those of the Poynting vector and local slowness methods.

INTRODUCTION

Determining the propagation directions of waves can be used in several seismic applications, such as constructing angle-domain common-image gathers (ADCIGs), which are used for velocity analysis (Biondi and Symes, 2004) and extracting amplitude variation with angle (AVA) information (Yan and Xie, 2012b); attenuating backscatter artifacts in reverse time migration (RTM) (Costa et al., 2009); and illumination analysis (Yang et al., 2008). Some of these applications require only scattering angles, which could also be calculated using techniques such as the image-domain common image gather technique of Sava and Fomel (2003). Calculating the time-domain propagation directions of the source and receiver waves separately provides additional information. This makes it possible, for example, to determine which side an interface is imaged from (Richardson and Malcolm, 2014).

Ray tracing simulations of wave propagation naturally provide propagation directions, but suffer from the inaccuracies resulting from the inherent high-frequency assumption (Gray et al., 2001). Finite-difference time stepping, often used in implementations of the seismic imaging method RTM (Baysal et al., 1983), allows closer adherence to the physics of finite-frequency wave propagation, but lacks a means of easily extracting propagation directions. Methods have been proposed for extracting directional information from finite-frequency wave-propagation schemes. One of these is the Poynting vector method (Yoon and Marfurt, 2006), which is computationally efficient, but it makes the assumption that the wavefield does not contain overlapping waves propagating in different directions (Patrikeeva and Sava, 2013). Another is the local slowness method (Xie et al., 2005), which does allow overlapping waves, but suffers from low angular resolution, as we demonstrate in the "Results" section (in particular in Figures 10 and 11). In this paper, we propose modifications of these two methods to mitigate these deficiencies.

The notion that waves have a particular propagation direction is only strictly true for waves of infinite frequency, or plane waves in a constant velocity medium. Our results are therefore distributions of amplitude as a function of direction, rather than vectors.

We start by describing the Poynting vector and local slowness methods. Following this, we explain the modifications that we propose to apply to them, primarily consisting of the addition of a wavefront orientation separation step, to enhance the ability to separate overlapping waves. Finally, we examine the effectiveness of the new methods compared with the Poynting vector and local slowness methods using simple examples to highlight the key improvements of the methods, and an example using the SEG Ad-

Manuscript received by the Editor 7 November 2014; revised manuscript received 17 December 2015; published online 19 April 2016.
[1]Formerly Massachusetts Institute of Technology, Department of Earth, Atmospheric, and Planetary Sciences, Cambridge, Massachusetts, USA; presently Ausar Geophysical, Dalkey, Ireland. E-mail: arichar@tcd.ie.
[2]Memorial University of Newfoundland, Department of Earth Sciences, St. John's, Newfoundland and Labrador, Canada. E-mail: amalcolm@mun.ca.

vanced Modeling (SEAM) model to demonstrate the robustness of the proposed methods to more complicated wavefields.

PREVIOUSLY PROPOSED METHODS

Poynting vectors

The Poynting vector method of determining wave-propagation direction was proposed by Yoon and Marfurt (2006) as a means of determining apparent scattering angle. It is not limited to calculating scattering angle, and so it may also be used in applications in which the propagation directions of the source and receiver wavefields must be known independently, such as in illumination compensation (Yang et al., 2008).

The Poynting vector method calculates the propagation direction $\hat{\boldsymbol{\psi}}$ at a point $\mathbf{x}$ and time t of wavefield u using

$$\hat{\boldsymbol{\psi}}(\mathbf{x},t;u) = -\frac{\partial u(\mathbf{x},t)}{\partial t}\nabla u(\mathbf{x},t)\left|\frac{\partial u(\mathbf{x},t)}{\partial t}\nabla u(\mathbf{x},t)\right|^{-1}, \quad (1)$$

where ∇ denotes the spatial gradient.

The method assumes that there are no overlapping waves (Patrikeeva and Sava, 2013), so the method assigns the full amplitude at each point in spacetime to a single propagation direction.

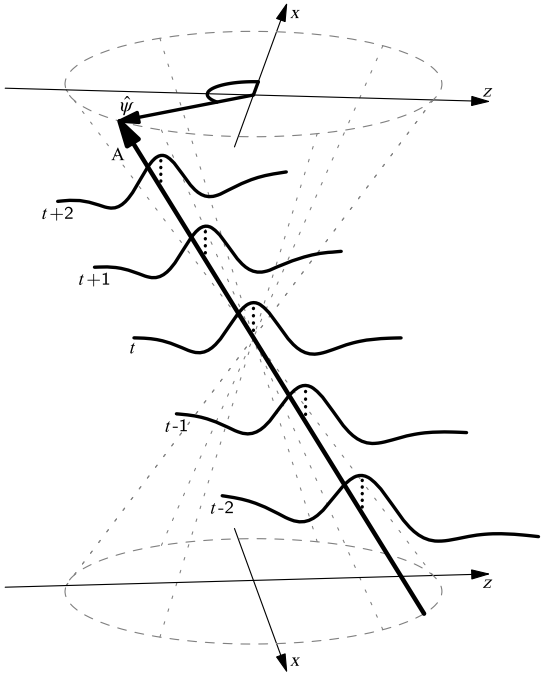

Figure 1. In two spatial dimensions, a wave propagating in direction $\hat{\boldsymbol{\psi}}$ and centered at the origin at time step t will travel along path A. Summing along A and dividing by the summation length, to apply the local slowness method, will therefore yield the value of the wave at its central peak. The circles represent the top and bottom edges of the light cone that the wave travels along. The dashed lines joining the two circles indicate the shape of the light cone. Summing along any other line on this cone other than A will yield zero, as long as the summation time is sufficiently long.

Local slowness

An alternative approach, called the local slowness method, was proposed by Xie et al. (2005). This method was initially developed to analyze near-source energy partitioning, but it has also been applied to determining propagation directions for illumination compensation (Xie and Yang, 2008) and constructing ADCIGs (Yan and Xie, 2012a). The method calculates the mean amplitude along potential propagation paths in spacetime. If a wave located at position $\mathbf{x}$ at time t, is propagating in direction $\hat{\boldsymbol{\psi}}$, and the local wave speed $c(\mathbf{x})$ is approximately constant, the wave travels along the "light cone" path in spacetime:

$$w(t',\mathbf{x},\hat{\boldsymbol{\psi}},t) = \mathbf{x} + \hat{\boldsymbol{\psi}}c(\mathbf{x})(t'-t). \quad (2)$$

For a particular $\hat{\boldsymbol{\psi}}$, the path w in two spatial dimensions is represented by line A in Figure 1. The mean along such a path is assumed to be the wave amplitude propagating in that direction:

$$u_s(\mathbf{x},\hat{\boldsymbol{\psi}},t) = \sum_{t'=-\frac{I_t}{2}}^{\frac{I_t}{2}} \frac{u(w(t',\mathbf{x},\hat{\boldsymbol{\psi}},t),t')}{I_t}, \quad (3)$$

where u_s is the wavefield containing only waves propagating in direction $\hat{\boldsymbol{\psi}}$, and I_t is the time over which the mean is calculated.

Calculating the mean along the local slowness direction, as shown in Figure 1 (line A), will sum the same part of the waveform at each time step, whereas calculating the mean in other directions will sample a different part of the waveform at each time step, leading to cancellation due to the oscillatory nature of waves and therefore a small amplitude. In contrast to the Poynting vector method, this approach is capable of separating a wavefield even when it contains overlapping waves propagating in different directions. The separation of overlapping waves is exact for plane waves in a constant velocity medium if the time over which the mean is calculated, I_t, is sufficiently large, but when these assumptions are violated, overlapping waves can still cause incomplete separation. Reducing the window size reduces the distance over which the assumptions must hold, but this decreases angular resolution (Yan and Xie, 2012a).

The summation is centered on time step t rather than summing from $t - I_t$ to t so that the spatial distance from $\mathbf{x}$ is minimized, reducing the likelihood of changes in wave speed along the light cone from $c(\mathbf{x})$.

MODIFIED METHODS

In this section, we propose modifications to the Poynting vector and local slowness methods. The modifications primarily consist of preceding the methods by a separation of the wavefields by wavefront orientation, so we first discuss techniques by which this may be achieved. The proposed modification allows the Poynting vector method to separate overlapping waves and enhances the angular resolution of the local slowness method. We assume that wave propagation occurs in isotropic, nonattenuating media. A simple extension to anisotropic materials is possible by simply using the anisotropic parameters to estimate the correct angle between the propagation direction and the wavefront; an understanding of how effective this approach would be in anisotropic media requires further research.

Wavefront orientation separation

The orientation of a wavefront $\hat{\boldsymbol{\psi}}$ is the direction of its gradient. In isotropic media, waves travel parallel to their wavefront orientation (i.e., the wavefront is perpendicular to the ray). A wavefront with orientation $\hat{\boldsymbol{\psi}}$ must therefore belong to a wave propagating in direction $\hat{\boldsymbol{\psi}}$ or $-\hat{\boldsymbol{\psi}}$. For locally planar waves, the wave amplitude is locally constant perpendicular to $\hat{\boldsymbol{\psi}}$, and oscillatory parallel to it. Direction $\hat{\boldsymbol{\psi}}$ is depicted in Figure 1.

The separation into wavefront orientation angles can be accomplished by several means, including through the use of the Fourier transform (Embree et al., 1963; Bamberger and Smith, 1992; Yilmaz, 2001), the curvelet transform (Candès et al., 2006), and time-domain local slant stack (LSS) (Durrani and Bisset, 1984; Yilmaz, 2001). We describe only the last of these because it has the advantage of being easily applied at specific locations. We will use this to reduce computational cost by only performing wavefront orientation separation where it is needed. A description of the other approaches can be found in Richardson (2015).

Local slant stack

LSS uses the fact that locally planar waves are oscillatory perpendicular to the wavefront and approximately constant along it. Summing along a wavefront in space will yield a nonzero value. Any direction not parallel to the wavefront should sum to zero because of the waves' oscillations, if the summation length is sufficiently long. This is shown in Figure 2. For a finite summation length, a wavefront will affect the mean calculated along nearby directions, as shown in Figure 2b. The magnitude of this effect is proportional to the time over which the wave is oscillatory, and it is inversely proportional to the summation length. The shortest time over which the wave is oscillatory depends on the source wavelet. It may be the duration of the wavelet or the period if the wave is periodic. Even if the wave is not periodic, if it has a single dominant frequency, we expect the wave to be close to oscillatory over the corresponding period. If the time period over which the pulse is oscillatory (or almost oscillatory) is T, then the corresponding spatial length is $c(\mathbf{x})T$ in the direction of propagation, where c is the wave speed, which we assume does not vary significantly over this distance. To separate a wavefront from a perpendicular wavefront also centered at $\mathbf{x}$, we therefore need to calculate the mean along the wavefront over the distance $[-(c(\mathbf{x})T)/2 : (c(\mathbf{x})T)/2]$ in 2D, or over the plane with sides of the same length along the wavefront in 3D, around the point $\mathbf{x}$. This is depicted in Figure 3 for the 2D case. To separate wavefronts that are not perpendicular, or not centered on $\mathbf{x}$, we would need to calculate the mean over a larger distance. Our assumptions about the planar nature of the wavefront and the locally constant velocity are less likely to be valid at larger distances, however. We therefore suggest using the shortest summation length in the mean calculation that will allow the amplitude along a wavefront to be determined without interference from wavefronts that are centered at $\mathbf{x}$ and oriented in any of the other directions to be considered. This will result in the angular spacing between the directions in which the summation is calculated being equal to the width of the distribution around $\hat{\boldsymbol{\psi}}^{\perp}$ in Figure 2b. Wavefronts oriented along a summation direction will therefore not leak into the mean calculated along neighboring summation directions. The amplitude related to wavefronts oriented between summation directions will be split between two calculated means. As depicted in Figure 4, for a given angular spacing between summation directions $\Delta\psi$, this requires a summation length of

$$I_{\mathbf{x}} = \frac{c(\mathbf{x})T}{\sin(\Delta\psi)}. \tag{4}$$

For a 2D wavefield decomposed into $N_s(t)$ equally spaced wavefront orientations (which will allow us to separate into $2N_s(t)$ propagation directions later), this is

$$\Delta\psi = \frac{\pi}{N_s(t)}. \tag{5}$$

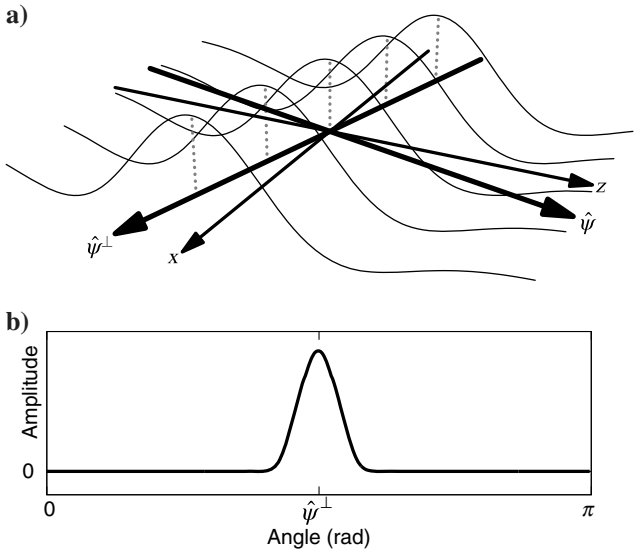

Figure 2. (a) A wavefront in space that is oscillatory in direction $\hat{\boldsymbol{\psi}}$ and constant in direction $\hat{\boldsymbol{\psi}}^{\perp}$. To perform wavefront orientation angle separation at the origin point in the figure, we compute the mean amplitude along lines passing through the origin. (b) The mean amplitude as a function of direction. Calculating the mean along the line pointing in direction $\hat{\boldsymbol{\psi}}^{\perp}$ in panel (a) will produce the peak value of the wave, whereas calculating the mean along the perpendicular line in direction $\hat{\boldsymbol{\psi}}$ will result in zero.

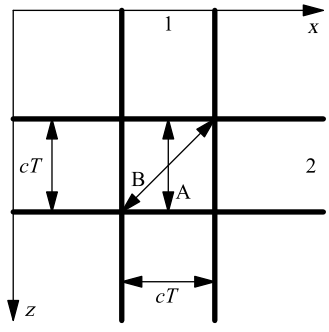

Figure 3. Waves 1 and 2 have perpendicular wavefront orientations. Both are oscillatory over the distance cT, where c is the local wave speed. The mean along A will be the value of wave 1 along that line with no interference from wave 2. The mean along line B will be zero.

In 3D, a geodesic grid may be used to distribute the chosen number of propagation directions into which the wavefield is decomposed over a sphere (Sahr et al., 2003).

The angular resolution $\Delta\psi$ obtainable with this method is approximately inversely proportional to $I_{\mathbf{x}}$ when $\Delta\psi$ is small. The maximum possible length $I_{\mathbf{x}}$ is determined by the distance over which the approximations of the method are valid. This depends on a number of factors such as the curvature of the wavefront, which will limit the locally planar wavefront assumption, and the smoothness of the model, which affects the distance over which the wave speed can be estimated as being constant. Increasing $I_{\mathbf{x}}$ beyond the length over which the assumptions hold will result in incorrect separated amplitude. This is because the foundational concepts of obtaining the amplitude of the wavefront when taking the mean perpendicular to the wavefront orientation, and obtaining zero when taking the mean over a sufficiently large distance that is not perpendicular to the wavefront orientation, will no longer be true. Angular resolution is approximately proportional to $c(\mathbf{x})T$, the product of the local wave speed and the shortest oscillatory time of the waves. Although it is a spatial quantity, in practice, the summation length is often specified as the summation time I_t because $I_{\mathbf{x}} = I_t c(\mathbf{x})$ varies in space with $c(\mathbf{x})$.

To separate the wavefield into waves with different wavefront orientation angles with LSS, we calculate the mean perpendicular to different wavefront orientations at each point $\mathbf{x}$:

$$u_o(\mathbf{x}, \hat{\boldsymbol{\psi}}, t) = \overline{u(\mathbf{x} + s(\hat{\boldsymbol{\psi}}, I_{\mathbf{x}}), t)}, \tag{6}$$

where $\bar{u}$ denotes the mean, $s(\hat{\boldsymbol{\psi}}, I_{\mathbf{x}})$ is a surface centered on the origin, normal to $\hat{\boldsymbol{\psi}}$, of spatial dimension one less than that of the wavefield, and of width $I_{\mathbf{x}} = I_t c(\mathbf{x})$ in each of its dimensions, u is the full wavefield, and u_o is the scalar field containing the amplitude of waves with wavefront orientation $\hat{\boldsymbol{\psi}}$ at position $\mathbf{x}$ and time t. If u is not defined at spatial locations requested by this mean, interpolation may be used.

Method 1: Modified Poynting vector method

We wish to determine the propagation directions and amplitudes of the $N(\mathbf{x}, t)$ waves passing through the point $\mathbf{x}$ at time t. If $\max(N) \leq 1$, the Poynting vector method works well and is computationally efficient; however, it fails when $N > 1$.

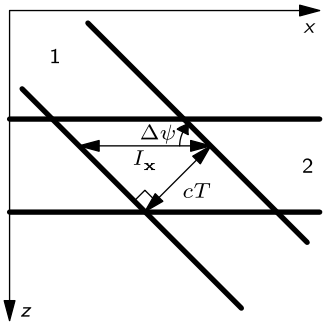

Figure 4. When the difference between the wavefront orientation angles of waves 1 and 2 is $\Delta\psi$, it is necessary to sum at least a distance $I_{\mathbf{x}}$ along wave 2 to cancel contributions from wave 1, where $I_{\mathbf{x}}$ is given by equation 4.

In this modified method, we separate the wavefield into waves with different wavefront orientations and apply two filters, based on the Poynting vector method, to determine the propagation directions.

By separating the wavefield by wavefront orientation $\hat{\boldsymbol{\psi}}$, we hope that

$$\max(N'(\mathbf{x}, \hat{\boldsymbol{\psi}}, t)) \leq 1, \tag{7}$$

where N' is the number of waves passing through the point $\mathbf{x}$ at time t that have a wavefront at point $\mathbf{x}$ oriented parallel to $\hat{\boldsymbol{\psi}}$. If this condition is satisfied, then we may successfully apply the Poynting vector method for the separated wavefield consisting of waves with wavefront orientation $\hat{\boldsymbol{\psi}}$, avoiding the problem of overlapping waves. Because the wavefront orientation separation will not separate two overlapping waves propagating in opposite directions $\hat{\boldsymbol{\psi}}$ and $-\hat{\boldsymbol{\psi}}$, as both have the same wavefront orientation $\hat{\boldsymbol{\psi}}$, the condition 7 can never be satisfied in this case. This method is therefore incapable of separating overlapping waves propagating in opposite directions.

Performing this separation on a sufficient number of time steps to calculate a time derivative (at least two), we calculate the Poynting vectors for each separated wavefront orientation, $\hat{\boldsymbol{\psi}}_p(\mathbf{x}, t; u_o(\mathbf{x}, \hat{\boldsymbol{\psi}}, t))$, using equation 1, and the apparent wave-propagation speed using

$$c_a(\mathbf{x}, \hat{\boldsymbol{\psi}}, t) = \left| \frac{\partial u_o(\mathbf{x}, \hat{\boldsymbol{\psi}}, t)}{\partial t} \left(\frac{\partial u_o(\mathbf{x}, \hat{\boldsymbol{\psi}}, t)}{\partial \hat{\boldsymbol{\psi}}} \right)^{-1} \right|. \tag{8}$$

The calculated propagation speed will be incorrect near the peaks and troughs of the wave because the spatial derivative at these locations will be close to zero, making the result unstable. We therefore apply smoothing by replacing the calculated speed at each point with its mean in a local neighborhood, weighted by the absolute value of the spatial derivative of $u_o(\mathbf{x}, \hat{\boldsymbol{\psi}}, t)$.

Because wavefront orientations $\hat{\boldsymbol{\psi}}$ and $-\hat{\boldsymbol{\psi}}$ are equivalent,

$$u_o(\mathbf{x}, \hat{\boldsymbol{\psi}}, t) = u_o(\mathbf{x}, -\hat{\boldsymbol{\psi}}, t). \tag{9}$$

The Poynting vectors $\hat{\boldsymbol{\psi}}_p$ and $-\hat{\boldsymbol{\psi}}_p$, and the apparent wave speeds $c_a(\mathbf{x}, \hat{\boldsymbol{\psi}}, t)$ and $c_a(\mathbf{x}, -\hat{\boldsymbol{\psi}}, t)$, can therefore all be computed using $u_o(\mathbf{x}, \hat{\boldsymbol{\psi}}, t)$.

If a wave is propagating in direction $\hat{\boldsymbol{\psi}}$, then $\hat{\boldsymbol{\psi}}_p$ should point in the same direction if the medium is isotropic. We also know that the wave-propagation speed should be $c(\mathbf{x})$. We exploit this to determine whether the wave with wavefront orientation $\hat{\boldsymbol{\psi}}$ is propagating in direction $\hat{\boldsymbol{\psi}}$ or $-\hat{\boldsymbol{\psi}}$, to enhance angular resolution, and to attenuate artifacts caused by violations of the method's assumptions (such as that the wavefield does not contain overlapping waves propagating in opposite directions). To achieve this, we calculate two filters. The first deals with the propagation direction:

$$\text{filt}_{\text{ang}}(\mathbf{x}, \hat{\boldsymbol{\psi}}, t) = (1 - \arccos(|\hat{\boldsymbol{\psi}}_p \cdot \hat{\boldsymbol{\psi}}|)/\pi)^d, \tag{10}$$

where d is a parameter to adjust how severely errors are treated. This expression computes the angular distance between the propagation direction $\hat{\boldsymbol{\psi}}_p$ determined with the Poynting vector method, and direction $\hat{\boldsymbol{\psi}}$, determined in the preprocessing wavefront orientation separation step. If the distance is zero, the filter has value one.

If the propagation direction is the opposite to the assigned direction, the filter has value zero. We found $d = 100$ to be effective, and used this in the presented results unless otherwise specified.

For the second filter, we penalize departures of the apparent wave speed from the actual wave speed:

$$\text{filt}_c(\mathbf{x}, \hat{\boldsymbol{\psi}}, t) = 1 - \min(|c(\mathbf{x}, t) - c_a(\mathbf{x}, \hat{\boldsymbol{\psi}}, t)|/\text{maxerror}, 1), \tag{11}$$

where maxerror is the maximum permissible error in c, for example, 1000 m/s (which we used for the results, unless otherwise specified).

The effect of these two filter parameters is examined in the "Results" section.

To obtain the wavefield separated by propagation direction, we multiply the wavefield separated by wavefront orientation with the two filters:

$$u_s(\mathbf{x}, \hat{\boldsymbol{\psi}}, t) = u_o(\mathbf{x}, \hat{\boldsymbol{\psi}}, t)\text{filt}_{\text{ang}}(\mathbf{x}, \hat{\boldsymbol{\psi}}, t)\text{filt}_c(\mathbf{x}, \hat{\boldsymbol{\psi}}, t). \tag{12}$$

This gives the final output $u_s(\mathbf{x}, \hat{\boldsymbol{\psi}}, t)$ of the modified Poynting vector method.

Method 2: Modified local slowness

Although the local slowness method is already capable of separating overlapping waves, preceding its application by a wavefront orientation step improves the achievable angular resolution.

The motivation for developing this modified method can be seen in Figure 5. Wavefront orientation separation has better angular resolution than the local slowness method for small differences in propagation direction, but its inability to distinguish between waves propagating in opposite directions means that it has poor resolution for large differences in propagation angle, the regime in which the resolution of the local slowness method is highest. By combining both methods, we derive the benefits of wavefront orientation separation's good resolution at small angles, while also retaining the local slowness method's ability to separate waves with large propagation angle differences.

Wavefronts along the path in equation 2 that are propagating in direction $\hat{\boldsymbol{\psi}}$ or $-\hat{\boldsymbol{\psi}}$ should have a wavefront orientation of $\hat{\boldsymbol{\psi}}$. To apply this last observation, we modify equation 3 to use the output of wavefront orientation separation u_o

$$u_s(\mathbf{x}, \hat{\boldsymbol{\psi}}, t) = \sum_{t'=-\frac{I_t}{2}}^{\frac{I_t}{2}} \frac{u_o(w(t', \mathbf{x}, \hat{\boldsymbol{\psi}}, t), \hat{\boldsymbol{\psi}}, t')}{I_t}. \tag{13}$$

An advantage of this approach over method 1 is that it is able to distinguish between overlapping waves propagating in opposite directions (which is not possible in method 1 due to the violation of equation 7). The memory requirement may be higher, however, because it is necessary to store the entire wavefield for more than the minimum of two time steps needed for method 1.

Including the wavefront orientation separation step increases the computational cost of the method compared with the original local slowness approach, but it improves the method's ability to distinguish between waves with small differences in propagation direction. This is explored in Appendix A, where we show, for example, that separating waves with propagation directions differing by $\pi/6$ rad requires $I_t = (4 + 2\sqrt{3})T \approx 7.5T$ when using the local slowness method, but only $I_t = (1 + \sqrt{3})T \approx 2.7T$ with method 2. This means that for the local slowness method to have sufficient angular resolution to separate such waves, the assumptions of the method must hold over a larger distance from the point being separated.

Method 2 could be further extended to include filters similar to those used in method 1, but this would further increase the computational cost of the method, which, as we show in the "Performance" subsection below, is already significant.

Performance

Although the proposed methods are more robust than the regular Poynting vector method, this comes at a substantial computational cost. The runtime and peak memory needed to decompose a 200 × 200 cell wavefield into 10 propagation directions with an oscillatory time T of 0.085 s, are presented in Figures 6 and 7, respectively. For runtime measurements, we compare the following:

1) For method 1, the runtime is that needed to perform wavefront orientation separation on two adjacent time slices and apply the Poynting vector method between them.
2) For method 2, it is assumed that the wavefront orientation separation has been done and the result stored for all but the final time step. The runtime for method 2 therefore includes only the time needed for the wavefront orientation separation of one time slice, and the sum over time slices.
3) For the Poynting vector and local slowness methods, the measured time is that needed to produce the separated wavefields for a single time step.

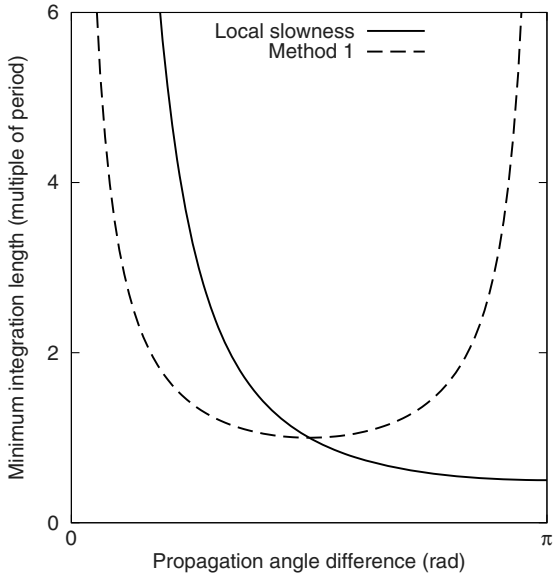

Figure 5. To separate waves propagating in directions differing by less than $\pi/2$, wavefront orientation separation requires a shorter summation length than the local slowness method (measured in the plot as a multiple of the time over which the waves are oscillatory, T, for the local slowness method, or $c(\mathbf{x})T$ for wavefront orientation separation). For larger differences in propagation direction, the local slowness method has better resolution for a given summation length. This plot is derived from equations in Appendix A.

We see that, in our implementation, the proposed methods require about twice the runtime of the local slowness method, and several times that of the Poynting vector method. Method 2 needs to store many time slices separated by wavefront orientation, whereas method 1 only needs to store two, the memory requirement of method 2 is only about three times that of method 1. This is because a large amount of memory is used to construct and apply the filters in method 1. Both methods again require several times the memory of the Poynting vector method; however, the memory requirements of the local slowness method are comparable with those of method 1.

Indications of how these values will vary as the parameters of the separation are changed are presented in Tables 1 and 2.

The performance advantage of the Poynting vector method will be greater in 3D because the directions in which the mean needs to be calculated in the other methods will grow. Additionally, the number of cells involved in the mean used in the LSS implementation of wavefront orientation separation will be larger because this mean will be taken over a plane rather than a line.

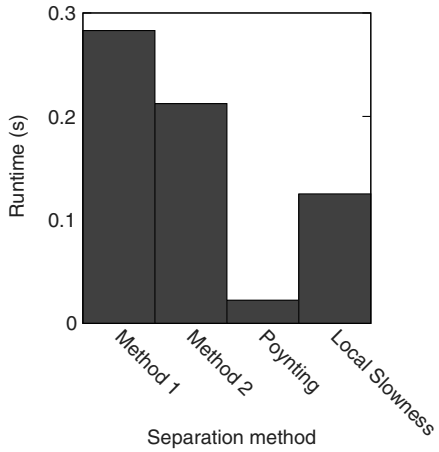

Figure 6. The time needed to perform directional separation on a single time slice of 200×200 cells, with $T = 0.085$ s and $\Delta t = 2.7 \times 10^{-4}$ s. For method 2, it is assumed that wavefront orientation separation has already been performed on all but the final time slice.

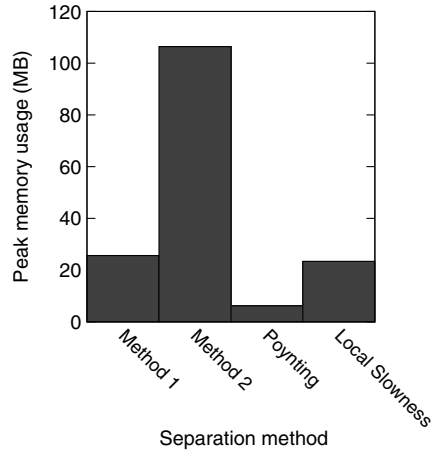

Figure 7. Memory required to perform the same separation as in Figure 6.

When multiple time steps are separated, the runtimes of all of the methods will scale linearly with the number of time steps, with the relative runtimes remaining the same. The memory usage needed for the computations will not increase.

All of the methods can be easily implemented efficiently on distributed memory computer clusters because most of the computations are spatially localized, and so little communication between computer nodes is required.

It is possible to reduce the additional cost of using the proposed methods by only applying them at locations where there are overlapping waves. At such locations, the assumption of the regular Poynting vector method that there is only one wave propagating at each grid point is violated, causing the method to return incorrect results (Patrikeeva and Sava, 2013). Elsewhere, where there are no overlapping waves, we can safely use the directions determined by the Poynting vector method, exploiting its efficiency. To determine where there are overlapping waves, and thus where the Poynting vector method is expected to fail, we use the fact that the Poynting vector method is based on the one-way wave equation:

$$c(\mathbf{x})\nabla u(\mathbf{x}, t) = -\partial_t u(\mathbf{x}, t). \tag{14}$$

At points where the Poynting vector method result is valid, meaning that there are no overlapping waves, equation 14 should be approximately equivalent to the two-way wave equation. This can be checked by calculating the apparent wave speed with equation 14:

$$c_a(\mathbf{x}) = \left| \frac{\partial_t u(\mathbf{x}, t)}{\nabla u(\mathbf{x}, t)} \right|. \tag{15}$$

Waves propagated with the two-way wave equation travel at the model wave speed $c(\mathbf{x})$, so if the one-way wave equation accurately describes the wave propagation at a point, the apparent wave speed (equation 15) and model wave speed should be the same. Where there is a large discrepancy, it means that the one-way wave equation is not a good approximation of the wave propagation, and thus,

Table 1. Computational complexity, where $N_{\mathbf{x}}$ is the number of cells in the discretized wavefield, N_p is the number of propagation directions that we wish to separate the wavefield into, I_t is the summation length in time, and n is the number of spatial dimensions.

Poynting vectors	$O(N_{\mathbf{x}})$
Local slowness	$O(N_{\mathbf{x}} N_p I_t)$
Method 1	$O(N_{\mathbf{x}} N_p I_t^{n-1} + N_{\mathbf{x}} N_p)$
Method 2	$O(N_{\mathbf{x}} N_p I_t^{n-1} + N_{\mathbf{x}} N_p I_t)$

Table 2. Memory requirements, where the symbols are described in Table 1.

Poynting vectors	$O(N_{\mathbf{x}})$
Local slowness	$O(N_{\mathbf{x}} I_t)$
Method 1	$O(N_{\mathbf{x}})$
Method 2	$O(N_{\mathbf{x}} N_p I_t)$

the Poynting vector result is unreliable. In cases where the Poynting vector method is expected to be successful over large portions of the wavefield, this enables the more expensive methods to be reserved for difficult areas. A similar filter was used by Dickens and Winbow (2011) to identify spurious Poynting vector results. As we show in the "Results" section below, even for a complicated wavefield, this can result in the proposed methods only needing to be applied to about half of the wavefield, with the efficient Poynting vector method used on the remainder. A similar approach could also be used to reduce the computational cost of the local slowness method.

A further reduction in the computational cost of the proposed methods could be achieved by using an initial guess of the propagation directions to decrease the number of directions in which the mean is calculated for wavefront orientation separation. This initial guess could be derived from the propagation directions found for a previous time step and from neighboring cells. If the sum of the amplitudes of waves with wavefront orientations in these initial guess directions is within a specified tolerance of the amplitude of the full wavefield at that location, summations to calculate the mean along other possible propagation directions are unnecessary.

RESULTS

In this section, we investigate the effects of the filter parameters for method 1, and compare the previously proposed Poynting vector and local slowness methods with the modified versions described in this paper. We then test the angular resolution under the idealized conditions of constant velocity, and demonstrate a deficiency of the Poynting vector method for computing ADCIGs. Finally, we compare the results on a complicated wavefield created by back-propagating receiver data through a 2D slice of the SEAM model. Because the angular resolution of the summation-based approaches (the local slowness method and methods 1 and 2) is limited by the summation distance, we choose I_x for each method, so that the maximum summation distance from the point being separated is the same for all of these methods.

The local slowness method uses points up to a distance $I_x/2$ from the point being separated in the direction of propagation (to calculate the mean along w in equation 3). Method 1 uses the same distance, but it is perpendicular to the direction of propagation (for the wavefront orientation separation). Method 2 combines the mean along the propagation direction of the local slowness method with wavefront orientation separation, and so it uses points up to $I_x/2$ in the direction of propagation and $I_x/2$ perpendicular to the direction of propagation from the separation point. For method 2, points up to $\sqrt{I_x^2/2^2 + I_x^2/2^2} = \sqrt{2}I_x/2$ (the hypotenuse of a triangle with sides of length $I_x/2$) distant are therefore involved. For a fair comparison, we therefore use a value of I_x for the local slowness method and method 1, which is $\sqrt{2}$ longer than that used for method 2.

Method 1 filter parameters

To examine the effect of the method 1 filter parameters d and maxerror, we consider the point on a wavefield, indicated by the arrow in Figure 8a. The wave was produced by a $\pi/3$ phase shifted 20 Hz Ricker wavelet source. Performing wavefront orientation separation at this point with a summation length of 0.085 s, and filter parameters $d = 2$ and maxerror $= 2000$, yields the AVA plot shown in Figure 8b. The wave is propagating in direction π rad (180°) from the reference angle, yet we can see that the summation length was not sufficient for this angle to be a peak of the absolute value of the amplitude as a function of angle. Figure 8c shows the effect on the location of the maximum peak of the absolute amplitude as the parameter for the propagation angle filter (d in equation 10) and the parameter for the apparent wave-speed filter (maxerror in equation 11) are adjusted. It is apparent that using a large angle filter parameter allows the correct angle to be the maximum peak at less stringent wave-speed filter parameter values. This is useful, as in Figure 8d we see that strong wave-speed filters (only allowing waves with a small error in apparent wave speed) can reduce amplitude accuracy. The inaccuracies in the calculation of apparent wave speed mean that we cannot expect a perfect match with the actual wave speed. Using filter values of 100 and 1000 for the angle and wave-speed filter, respectively, produces the result in Figure 8e, which has a peak at the correct angle and an amplitude at the peak within 14% of the true value.

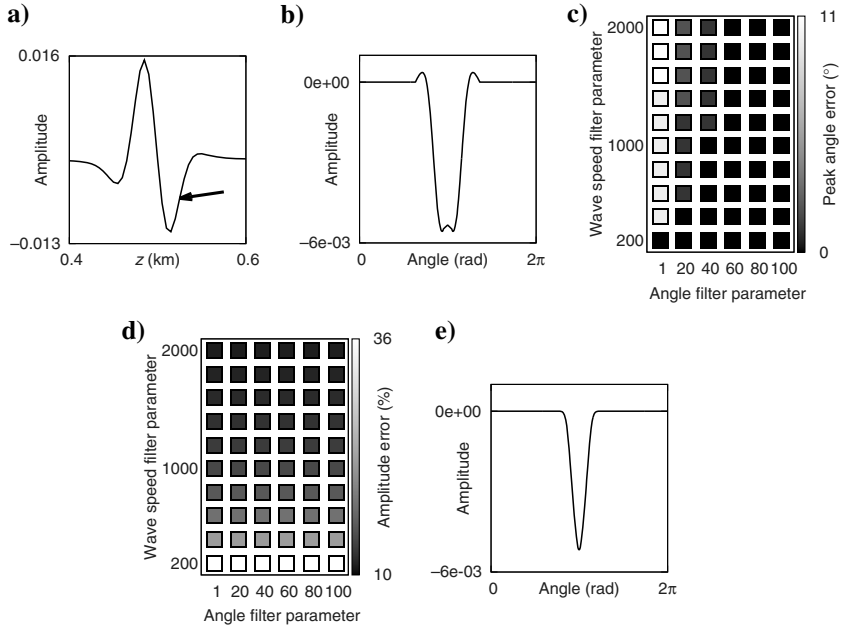

Figure 8. (a) The point on a wave propagating in direction π rad, which is used to investigate the effect of filter parameters in method 1. (b) With filter parameters $d = 2$ and maxerror $= 2000$, the true propagation direction (π rad) is not a peak of absolute amplitude. (c) The location of the maximum peak in absolute AVA varies with the choice of parameters for the method's two filters. (d) As in panel (c), but for relative amplitude error in the wave amplitude assigned to the true direction of propagation. (e) As in panel (b) but with filter parameters, $d = 100$ and maxerror $= 1000$. The peak occurs at the angle of the true propagation direction.

Crossing waves 1

To test the ability of the methods to separate overlapping waves, we create a wavefield using six sources arranged around a hemisphere of radius 750 m. The sources emit a 20 Hz Ricker wavelet, and the wave speed is constant everywhere at 1500 m/s. We attempt to separate the wavefield 0.5 s after the peak source input, as the six waves are crossing. (The unseparated wavefield at this time is shown in Figure 10a.) For method 1 and the local slowness method, we use 0.17 s, twice the duration of the source wavelet, as the summation time. Because the wave speed is constant, this corresponds to a spatial summation length of 255 m everywhere. According to equation 4, this allows method 1 to separate waves with propagation directions differing by at least 30° (which is the minimum difference between waves in the example wavefield) without interference. For method 2, we use a summation time of 0.12 s, as explained at the beginning of section "Results" ($0.17 = \sqrt{2} \times 0.12$).

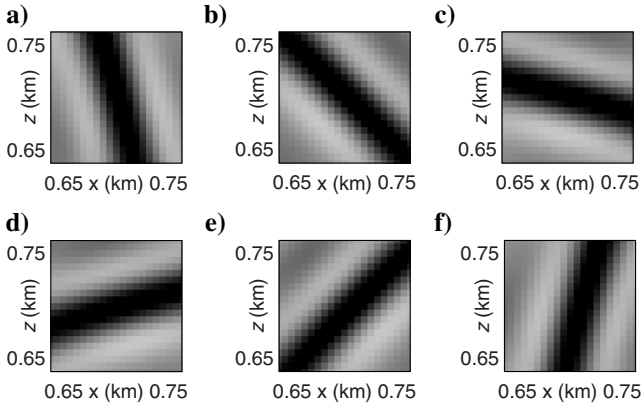

Figure 9. Wavefront orientation separation isolates the six overlapping waves in the wavefield depicted in Figure 10a.

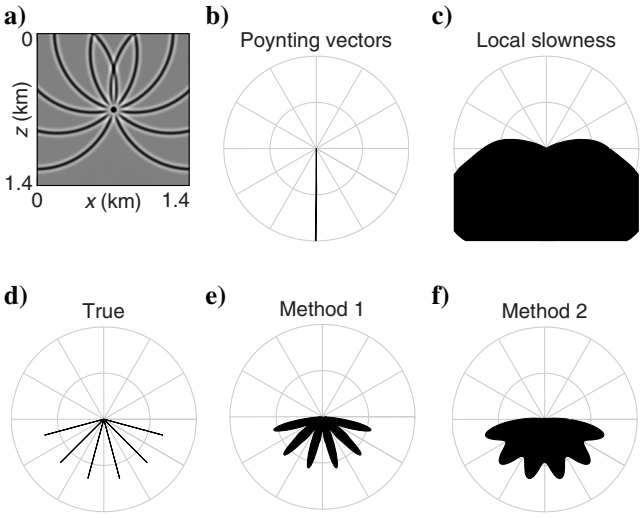

Figure 10. (a) A time slice of six waves overlapping obliquely. Directional separation is performed at the central point. (b-f) Results of directional separation on the wavefield in panel (a). Propagation angle is on the polar axis, whereas the radial axis represents amplitude. The displayed amplitude range is the same for all plots.

The output of wavefront orientation separation in the directions of the six wavefronts at one time step is shown in Figure 9. Only the central portion of the wavefield, where the waves overlap, is shown. The six waves have been successfully separated, allowing the Poynting vector method to be applied for method 1, or equation 13 for method 2, to determine the propagation directions without interference from other waves.

In Figure 10, we show the amplitude of waves determined by different methods to be propagating in each direction at the chosen point, where the waves from the six sources are overlapping. As expected, the Poynting vector method fails in this test because its assumption that waves do not overlap is violated. The peak angle of the local slowness method is similar to that of the Poynting vector method (not visible in the displayed figures due to clipping) because the angular resolution with the given summation time is not sufficient to distinguish between the six propagation directions. Both of the modified methods produce results that are quite close to the true separation. The angular resolution of the method 2 result is lower than that of method 1 due to the shorter summation time, as described above. If the crossing waves were plane waves, the angular resolution of the two proposed methods and the local slowness method could be improved by using a longer summation time. Because the wavefronts are curved in this example, the maximum summation length over which the plane-wave assumption of the methods is valid is limited, restricting achievable resolution, as previously discussed.

For demonstration purposes, we separated the wavefield into 360 1° propagation angle bins. This results in the smooth appearance of the output. Because, as indicated above, the summation lengths used mean that the minimum propagation angle difference that can be separated without interference is 30° for method 1, in practice one would normally use far fewer (on the order of 12 bins). Optimizing the directions of these bins, so that they occur at the peaks of the wavefront orientation separation function (direction $\hat{\boldsymbol{\psi}}^{\perp}$ in Figure 2b), would result in the output of the two proposed methods matching almost exactly with the true separation.

Crossing waves 2

To examine the effect of wavelet phase on the methods, we repeat the previous test, but use Ricker wavelets with phase shifts ranging from 0° to 90°. As described in the "Performance" subsection, we only apply the proposed methods in areas where the Poynting vector method is expected to fail due to the calculated apparent wave speed differing from the actual model wave speed by more than a chosen threshold. Figure 11a shows the full wavefield, and the regions where the proposed methods were applied due to the apparent wave speed differing by more than our chosen threshold of 100 m/s from the actual wave speed. The computationally efficient Poynting vector method was thus used on most of the wavefield, whereas the proposed methods were primarily reserved for the regions of the wavefield where there are crossing waves. The separation results for the central crossing point are shown in Figure 11. The Poynting vector and local slowness methods are again unable to distinguish the different propagation directions. The 90° phase shifted Ricker wave has zero amplitude at the central crossing point. The violation of the local plane-wave assumption in the two proposed methods by the curvature of the wavefronts in this example causes a small but nonzero amplitude to be assigned to the propagation direction of this wave. The proposed methods otherwise deliver results that closely match the true propagation amplitudes.

ADCIG

A common use for propagation direction separation is the construction of ADCIGs using the calculated scattering angles. The deviation of reflectors from horizontal lines as a function of angle is used in wave equation migration velocity analysis to determine velocity model updates. Inaccurate propagation direction information can therefore lead to incorrect updates. To demonstrate a situation in which this occurs with the Poynting vector method, we construct ADCIGs using a simple model consisting of a single reflector. Because we use the exact velocity model, a reflected wave is generated from the interface. This causes there to be overlapping waves, which interferes with correct propagation direction determination by the Poynting vector method. We highlight this in the result, shown in Figure 12, by plotting the scattering angle of the ADCIG to which each source contributes the peak amplitude as a function of surface offset between the source and the ADCIG location, at the depth of the interface. At large offsets, and thus large scattering angles, when the reflection coefficient of the interface is largest, the Poynting vector method result diverges from the analytical result, whereas the other methods continue to produce reliable scattering angle measurements.

SEAM

To investigate the behavior of the methods under less idealized conditions, we consider the back-propagated receiver wavefield for a single shot in a 2D slice of the SEAM model shown in Figure 13n. Directionally separating the back-propagated receiver wavefield like this can be used in many applications, such as generating ADCIGs and performing illumination compensation, but the complexity of the receiver wavefield means that the Poynting vector method is not well-suited to the task. The SEAM model was designed to provide a realistic test for imaging and inversion techniques (Fehler and Larner, 2008). We back propagate the data, produced with a 15 Hz Ricker wavelet source, using an acoustic propagator. We use a separation time of 0.266 s for the local slowness method and method 1, and 0.188 s for method 2.

Because we do not know the true directional decomposition of this wavefield, we can only judge the results on how visually plausible they appear. A selection of propagation directions of the resulting separated wavefields at a single time step is shown in Figure 13. Figure 13m shows the full wavefield at this time step. It is complicated, with several overlapping waves propagating in different directions. The selected propagation directions, 60° apart, are designated by the arrows in the top image in each column. The proposed methods were only used in regions where the Poynting vector result was likely to be inaccurate, as determined by the previously described criterion. In this example, the Poynting vector result was used for 45% of the wavefield, resulting in almost a 45% decrease in computational cost of the proposed methods.

In the left column of Figure 13, the almost horizontal wavefront A is clearly visible in the Poynting vector result despite propagating in a different direction to that chosen. It is also more prominent in the local slowness result than in either of the proposed methods. In the center column, this wavefront, now indicated by B, is less clearly visible in the Poynting vector result than in the left column, despite the propagation direction of the center column being closer to that of the wave. The other methods accurately separate this wave. In the right column, the worse angular resolution of the local slowness method compared with the proposed methods is apparent at the point indicated by C. The right column displays waves that are supposed to be traveling toward the top right, yet a wave that appears to be propagating toward greater depth has been assigned to this direction by the local slowness method. This wave is also visible in method 2, but has lower amplitude, and is absent from the separated wavefield produced by method 1. The weakness of the Poynting vector method is also seen in the right column because the wave near D is missing, despite propagating in a direction close to that selected.

DISCUSSION

The results of the tests presented indicate that neither the Poynting vector method nor the local slowness method can be used reliably to separate wavefields by propagation direction when there are overlap-

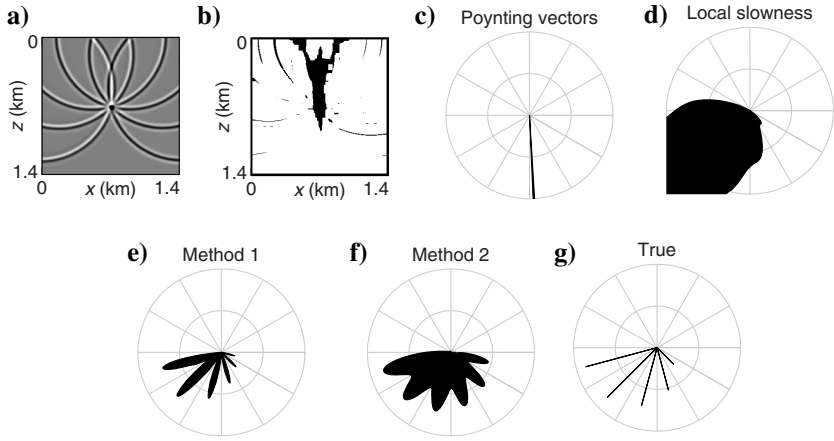

Figure 11. Directional separation on a wavefield with waves of different phases. (a) The full wavefield. (b) The portion of the wavefield (in black) where the proposed methods are applied due to the expected failure of the Poynting vector method. (c-g) Directional separation results, in the same style as Figure 10.

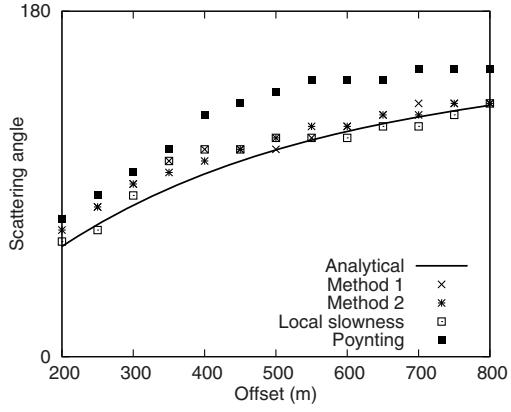

Figure 12. The peak amplitude angle as a function of surface offset along a reflector does not match the analytical result when using the Poynting vector method.

ping waves. Although neither of the modified methods performed flawlessly in all evaluations, they were generally superior.

We allude on several instances to the limits on achievable accuracy, which involve multiple factors. One of these is the frequency content of the wavefield, when the distance over which the wavefronts are planar is finite. Equation 4 demonstrates the diminishing ability to distinguish between wavefronts with different orientations as the frequency of the waves decreases. Similar results hold for the spacetime summation means of separation used in the local slowness method. Expressing the angular resolution limits of frequency on the Poynting vector approach is not as clear, but it is obvious that for low-frequency waves, the decreasing amplitude of the space and time derivatives will result in numerical errors becoming more prominent. Another factor affecting accuracy is the sampling of the wavefield in space and time. Using more information about the wavefield, as is done in method 2, increases potential accuracy, but for discretized, finite-frequency wavefields, there will always be limits to achievable angular resolution, regardless of the separation method used.

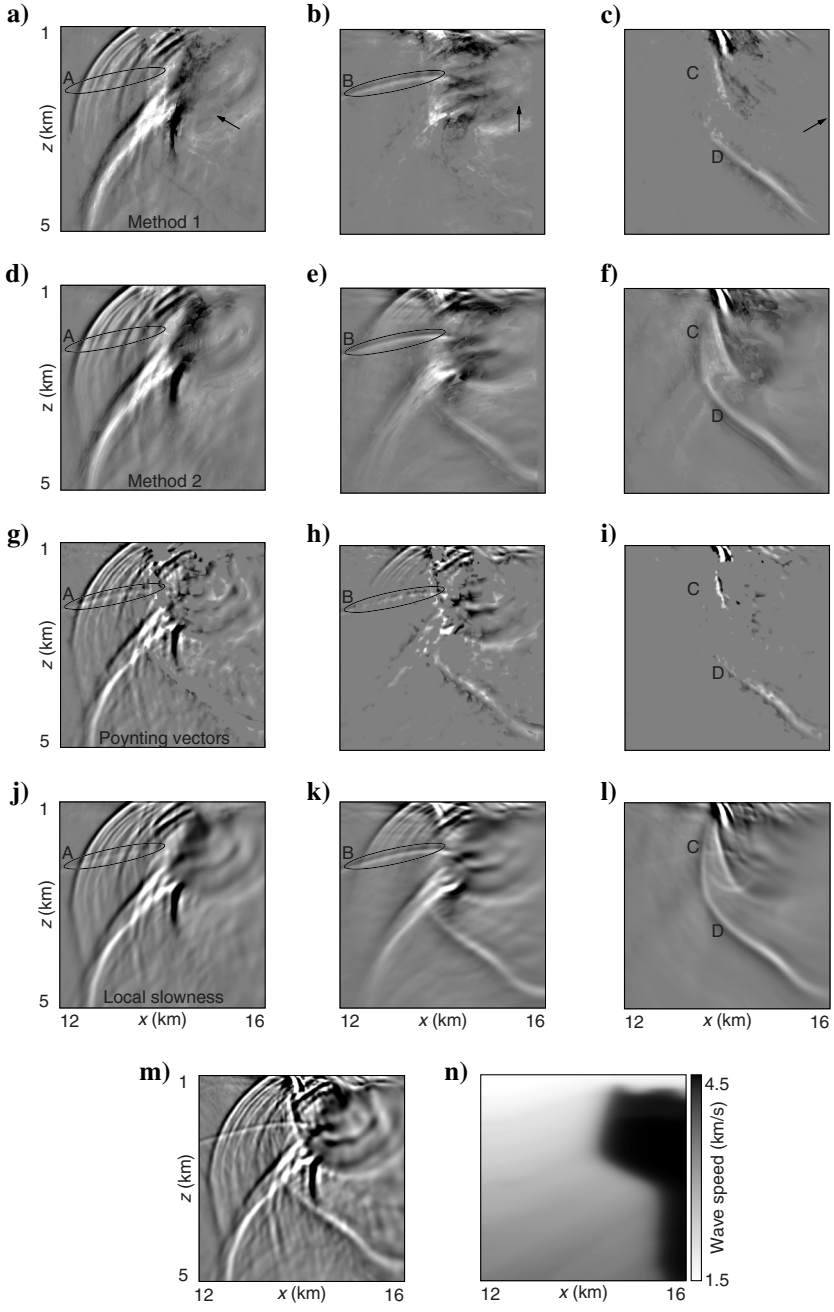

Figure 13. The back-propagated receiver wavefield generated by a shot at 0 m x and 15 m z. The full wavefield at one time step is shown in panel (m) and the velocity model in panel (n), whereas the other images (a-l) show only the waves propagating in the depicted directions (indicated by arrows in the top image of each column), as determined by different separation methods.

CONCLUSION

This paper presents modifications of the Poynting vector and local slowness methods for separating a wavefield into waves propagating in different directions. Unlike the previously proposed Poynting vector method, the modified version presented here is capable of performing the separation even when there are overlapping waves. The local slowness method is also able to do this, but, as we demonstrate, it has poorer angular resolution than the modified version we propose. Separating the wavefield by wavefront orientation, a key component of both of our modified methods, provides good angular resolution, enabling both methods to separate six overlapping waves when the Poynting vector and local slowness methods fail to do so. The proposed methods are significantly more computationally expensive than the Poynting vector method, and even the local slowness method. To avoid unnecessary computational expense, we restrict the application of our proposed methods to regions of the wavefield where the Poynting vector method is expected to fail due to incorrect wave speed calculated using the one-way wave equation on which it is based. Even on the complicated back-propagated SEAM receiver wavefield, this reduces the runtime of the proposed methods by almost half.

ACKNOWLEDGMENTS

The authors wish to thank Total for support and P. Williamson of Total for his useful suggestions. Three anonymous reviewers also helped to substantially improve the communication of our results.

APPENDIX A

RESOLUTION OF METHOD 2 AND THE LOCAL SLOWNESS METHOD

In this appendix, we investigate the differences in angular resolution between method 2 and the local slowness method with the aid of Figure A-1. This depicts a wave propagating toward the bottom of the page (wave 1, $\hat{\boldsymbol{\psi}}_1 = \widehat{\pi/2}$, where $\widehat{\pi/2}$ is a

unit vector in the direction that makes an angle of $\pi/2$ with the positive x-axis), which is oscillatory over time T, and therefore also over the distance cT (where c is the local wave speed). We show the location of wave 1 at time step $t + I_t/2$. It is assumed to be a plane wave, constant parallel to the wavefront. O is the point on wave 1 that will be at the location being separated at time step t. At time t, this point on wave 1 will therefore have propagated to the center of the dashed semicircle. The semicircle represents half of the top of the light cone that is visible in Figure 1. The local slowness summation in the direction pointing downward from the separation point would add the amplitude of the wave at the point O at each time step. So, as long as there was no interference from overlapping waves, after dividing by the number of summed time steps, the local slowness method would correctly say that a wave with the amplitude of the point O was propagating downward. Method 2 would obtain the same result. The difference between method 2 and the local slowness method becomes apparent when considering the minimum angular distance between the propagation directions of this wave (wave 1) and an overlapping wave (wave 2), such that the amplitudes assigned to the propagation directions of the two waves in the methods' output are correct. We will assume that wave 2 is also oscillatory over a distance cT. These amplitudes will be correct if, when the method calculates the mean along the propagation direction of one wave (which, without loss of generality, we take to be wave 2), it includes in the mean all points along the propagation direction of wave 1 over its oscillatory distance cT (this will result in cancellation of wave 1). Here, we compute the minimum difference in propagation direction between waves 1 and 2, for this to be true for the local slowness method and method 2.

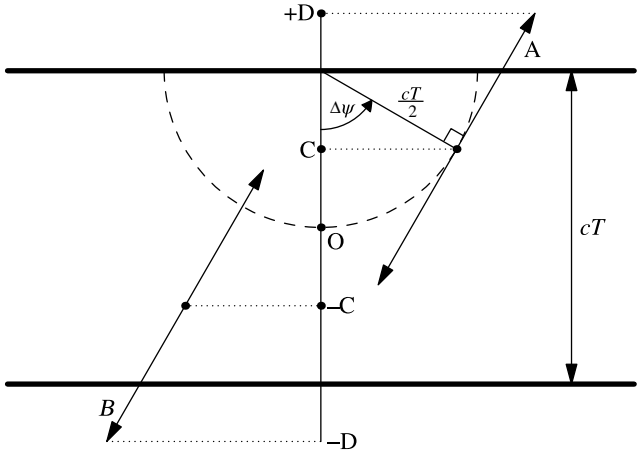

Figure A-1. A downgoing wave at time step $t + I_t/2$, oscillatory over the length cT. The horizontal axis represents x, whereas the vertical axis is z. The two thick, horizontal lines indicate the beginning and end of the wave packet. We depict the case when $I_{\mathbf{x}} = cT$ is used as the summation length for wavefront orientation angle separation, and $I_t = T$ is the summation time for the local slowness slant stack. O, C, and D are points on the wave, which move with the wave as it propagates. The values -C and -D are the mirrors of points C and D through point O, respectively. The semicircle shows half of the top edge of the light cone centered on time step t. At time step $t + I_t/2$, the LSS sum for wavefront orientation angle separation will be composed of the points of the wave along line A when the orientation of the wavefront being separated differs from that of the depicted wave by $\Delta\psi$. At time $t - I_t/2$, the summation points of the wave will be those along the line B. It may be useful to re-examine Figure 1 when considering this diagram.

To accomplish this, we determine the elements of wave 1 that are contained in the mean calculated along the propagation direction of wave 2, whose propagation direction differs from that of wave 1 by an angle $\Delta\psi$ ($\hat{\boldsymbol{\psi}}_2 = \widehat{\pi/2 + \Delta\psi}$). Although we choose wave 1 to be propagating downward for simplicity, the results are still valid if the two waves are rotated.

Local slowness method

For the local slowness method, we rewrite equation 3:

$$u_s^c[x, z, \hat{\boldsymbol{\psi}}_2, t] = \sum_{j=-I_t/2}^{I_t/2} \frac{1}{I_t} u[x + jc[x, z]\sin(\Delta\psi), z + jc[x, z]\cos(\Delta\psi), t + j], \tag{A-1}$$

where $u_s^c[x, z, \hat{\boldsymbol{\psi}}_2, t]$ is the amplitude determined to be propagating in direction $\hat{\boldsymbol{\psi}}_2$ at position (x, z) and time t, and the other symbols are as defined previously, in particular I_t is the number of time steps in the summation.

This sum will include the same value of wave 2 at each time step, but different elements of wave 1. We may therefore separate it into two terms:

$$u_s^c[x, z, \hat{\boldsymbol{\psi}}_2, t] = \sum_{j=-I_t/2}^{I_t/2} \frac{1}{I_t} (u_s[x, z, \hat{\boldsymbol{\psi}}_2, t] + u_s[x + jc[x, z]\sin(\Delta\psi), z + jc[x, z]\cos(\Delta\psi), \widehat{\pi/2}, t + j]), \tag{A-2}$$

$$u_s^c[x, z, \hat{\boldsymbol{\psi}}_2, t] = u_s[x, z, \hat{\boldsymbol{\psi}}_2, t] + \sum_{j=-I_t/2}^{I_t/2} \frac{1}{I_t} u_s[x + jc[x, z] \times \sin(\Delta\psi), z + jc[x, z]\cos(\Delta\psi), \widehat{\pi/2}, t + j], \tag{A-3}$$

where $u_s[x, z, \hat{\boldsymbol{\psi}}_2, t]$ is the true amplitude of wave 2, and $u_s[x, z, \widehat{\pi/2}, t]$ is the true amplitude of wave 1.

For the calculated amplitude to be correct, we require that

$$u_s^c[x, z, \hat{\boldsymbol{\psi}}_2, t] = u_s[x, z, \hat{\boldsymbol{\psi}}_2, t]. \tag{A-4}$$

For this to be true,

$$\sum_{j=-I_t/2}^{I_t/2} \frac{1}{I_t} u_s[x + jc[x, z]\sin(\Delta\psi), z + jc[x, z]\cos(\Delta\psi), \widehat{\pi/2}, t + j] = 0. \tag{A-5}$$

To relate this equation more directly to wave 1, we will replace the fixed reference frame with a reference frame moving downward with wave 1. Because wave 1 is assumed to be constant perpendicular to the propagation direction, we will also disregard the x coordinates, giving

$$\sum_{j=-I_t/2}^{I_t/2} \frac{1}{I_t} u_s[x, z + jc[x,z]\cos(\Delta\psi) - jc[x,z], \widehat{\pi/2}, t] = 0. \tag{A-6}$$

This sum is over values of the downgoing wave from the point -C (at time step $t - I_t/2$) to C (at time step $t + I_t/2$) in Figure A-1, where

$$\mathrm{C} = \mathrm{O} + \frac{cI_t}{2}(1 - \cos\Delta\psi)\hat{z}. \tag{A-7}$$

Points C and -C are symmetric about the point O rather than the center of the semicircle (even though summation along any direction on the light cone will indeed be symmetric about the center of the semicircle) because the figure shows the points on the downgoing wave that are included in the summation and the downgoing wave moves with time.

We know that wave 1 is oscillatory over time T, and therefore distance $c[x,z]T$, which implies that

$$\sum_{i=-c[x,z]T/2}^{c[x,z]T/2} u_s[x, z - i, \widehat{\pi/2}, t] = 0, \tag{A-8}$$

where we have assumed that wave 1 is either a wave packet of length $c[x,z]T$ and z is in the center of it, or is periodic.

Comparing equations A-6 and A-8 indicates that for A-4 to be true, we must have

$$I_t(\cos(\Delta\psi) - 1) = -T, \tag{A-9}$$

$$\Rightarrow \Delta\psi = \arccos\left(1 - \frac{T}{I_t}\right). \tag{A-10}$$

This is equivalent to the condition

$$2|\mathrm{C}| \geq cT. \tag{A-11}$$

If the waves have propagation directions separated by $\Delta\psi = \pi/6$, we therefore require that

$$\frac{I_t}{T} = 4 + 2\sqrt{3}. \tag{A-12}$$

Method 2

We will now follow a similar approach for method 2 using LSS for wavefront orientation separation. This involves a summation over space, to apply LSS, and the results of this are then summed in spacetime along the light cone. This gives

$$u_s^c[x, z, \hat{\boldsymbol{\psi}}_2, t] = \sum_{j=-I_t/2}^{I_t/2} \sum_{i=-c[x,z]I_t/2}^{c[x,z]I_t/2} \frac{1}{c[x,z]I_t^2} u[x + jc[x,z] \times \sin\Delta\psi + i\cos\Delta\psi, z + jc[x,z]\cos\Delta\psi - i\sin\Delta\psi, t + j] \tag{A-13}$$

for the calculated amplitude u_s^c, which is equivalent to

$$u_s^c[x, z, \hat{\boldsymbol{\psi}}_2, t] = \sum_{j=-I_t/2}^{I_t/2} \sum_{i=-c[x,z]I_t/2}^{c[x,z]I_t/2} \frac{1}{c[x,z]I_t^2} (u_s[x, z, \hat{\boldsymbol{\psi}}_2, t] + u_s[x + jc[x,z]\sin\Delta\psi + i\cos\Delta\psi, z + jc[x,z]\cos\Delta\psi - i\sin\Delta\psi, \widehat{\pi/2}, t + j]), \tag{A-14}$$

where, as in the local slowness calculation, we split the wavefield u into components from waves 1 and 2.

For $u_s^c[x, z, \hat{\boldsymbol{\psi}}_2, t] = u_s[x, z, \hat{\boldsymbol{\psi}}_2, t]$ to be true, we therefore require that

$$\sum_{j=-I_t/2}^{I_t/2} \sum_{i=-c[x,z]I_t/2}^{c[x,z]I_t/2} \frac{1}{c[x,z]I_t^2} u_s[x, z + jc[x,z] \times \cos\Delta\psi - i\sin\Delta\psi - jc[x,z], \widehat{\pi/2}, t] = 0. \tag{A-15}$$

At time step $t + I_t/2$, this spatial summation is along the line A, as shown in Figure A-1. At time step $t - I_t/2$, it will be along the part of the downgoing wave covered by the line B. As with the labeled points, these lines use the (moving) downgoing wave as a reference frame, rather than a fixed point in space. If a fixed point in space had instead been used, B would be the mirror of A through the center of the semicircle. The combination of these two summations will therefore cover the range of values of the downgoing wave from −D to D, where

$$\mathrm{D} = \mathrm{O} - \frac{cI_t}{2}(1 - \cos\Delta\psi + \sin\Delta\psi)\hat{z}. \tag{A-16}$$

Although equation A-15 cannot be directly related to equation A-8 due to the double summation, we see that for small values of $\Delta\psi$,

$$jc[x,z]\cos\Delta\psi - jc[x,z] \approx 0. \tag{A-17}$$

In this small angle regime, we can match equation A-8 when

$$I_t \sin\Delta\psi = T, \tag{A-18}$$

$$\Rightarrow \Delta\psi = \arcsin\left(\frac{T}{I_t}\right). \tag{A-19}$$

This is, in fact, the minimum difference in wavefront orientation between two waves that the LSS method can resolve, for a given T and I_t. It is therefore the angular resolution of method 1 using LSS when no filters are applied. As shown in Figure 5, at less than $\pi/2$, this angle is smaller for a given I_t (as a multiple of T) than the minimum angle resolvable with the local slowness method.

When $\Delta\psi$ is not small, the $jc[x,z](\cos\Delta\psi - 1)$ term is nonnegligible. If wave 1 is periodic, with period T, then as long as the LSS sum covers the distance cT in the direction of periodicity, shifting

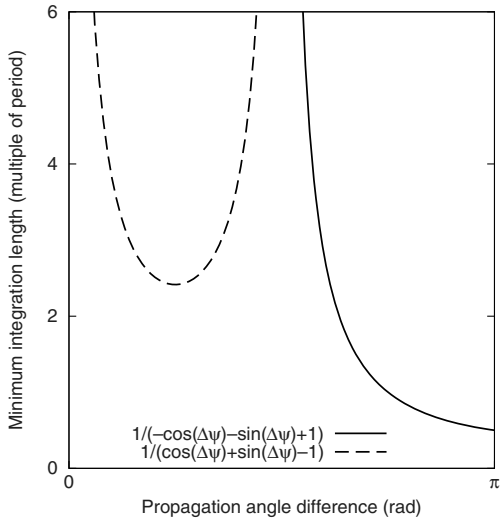

Figure A-2. Similar to Figure 5, but for method 2 when the waves are wave packets of duration T.

the sum in space, as occurs in equation A-15, does not affect the output. The condition in equation A-19 therefore still holds.

When wave 1 is not periodic, the sum in equation A-15 will in general include different z values of the wave different numbers of times. For example, in the situation depicted in Figure A-1, the value of the wave at O is included in the summation of every time step, whereas the value at +D is only included in the summation of time step $t + I_t/2$. Although some cancellation may take place, there is likely to be a nonzero remainder. If wave 1 is a wave packet that is only nonzero over a length cT in z, then we may ensure that the sum equates to zero by choosing I_t such that all of the nonzero z elements are included with an equal number of times in the sum. By inspection of Figure A-1, this can be achieved for $\Delta\psi \le \pi/2$ by requiring that

$$\frac{I_t}{T} \ge \frac{1}{\cos\,\Delta\psi + \sin\,\Delta\psi - 1}, \tag{A-20}$$

and for $\Delta\psi > \pi/2$ with the condition

$$\frac{I_t}{T} \ge \frac{1}{-\cos\,\Delta\psi - \sin\,\Delta\psi + 1}. \tag{A-21}$$

These equations are plotted in Figure A-2. The method is able to attain similar angular resolution to method 1 for small $\Delta\psi$, and to the local slowness method near $\Delta\psi = \pi$. It has difficulty when waves are propagating in directions separated by right angles, however. This is because when $\Delta\psi = \pi/2$, any choice of I_t will result in the value of wave 1 at O being included in the summation twice as many times as the values at the edges of the wave packet, and so full cancellation is not possible (but the result should still be small). Nevertheless, we see from the "Results" section that the method still appears to work effectively in many cases.

REFERENCES

Bamberger, R. H., and M. J. Smith, 1992, A filter bank for the directional decomposition of images: Theory and design: IEEE Transactions on Signal Processing, **40**, 882–893, doi: 10.1109/78.127960.

Baysal, E., D. D. Kosloff, and J. W. Sherwood, 1983, Reverse time migration: Geophysics, **48**, 1514–1524, doi: 10.1190/1.1441434.

Biondi, B., and W. W. Symes, 2004, Angle-domain common-image gathers for migration velocity analysis by wavefield-continuation imaging: Geophysics, **69**, 1283–1298, doi: 10.1190/1.1801945.

Candès, E., L. Demanet, D. Donoho, and L. Ying, 2006, Fast discrete curvelet transforms: Multiscale Modeling and Simulation, **5**, 861–899, doi: 10.1137/05064182X.

Costa, J., F. Silva Neto, M. Alcntara, J. Schleicher, and A. Novais, 2009, Obliquity-correction imaging condition for reverse time migration: Geophysics, **74**, no. 3, S57–S66, doi: 10.1190/1.3110589.

Dickens, T. A., and G. A. Winbow, 2011, RTM angle gathers using Poynting vectors: 81st Annual International Meeting, SEG, Expanded Abstracts, 3109–3113.

Durrani, T., and D. Bisset, 1984, The Radon transform and its properties: Geophysics, **49**, 1180–1187, doi: 10.1190/1.1441747.

Embree, P., J. P. Burg, and M. M. Backus, 1963, Wide-band velocity filtering — The pie-slice process: Geophysics, **28**, 948–974, doi: 10.1190/1.1439310.

Fehler, M., and K. Larner, 2008, SEG advanced modeling (SEAM): Phase I first year update: The Leading Edge, **27**, 1006–1007, doi: 10.1190/1.2967551.

Gray, S., J. Etgen, J. Dellinger, and D. Whitmore, 2001, Seismic migration problems and solutions: Geophysics, **66**, 1622–1640, doi: 10.1190/1.1487107.

Patrikeeva, N., and P. Sava, 2013, Comparison of angle decomposition methods for wave-equation migration: 83rd Annual International Meeting, SEG, Expanded Abstracts, 3773–3778.

Richardson, A., 2015, Seismic imaging using internal multiples and overturned waves: Ph.D. thesis, Massachusetts Institute of Technology.

Richardson, A., and A. E. Malcolm, 2014, Illumination compensation using Poynting vectors, with special treatment for multiples: 84th Annual International Meeting, SEG, Expanded Abstracts, 3956–3961.

Sahr, K., D. White, and A. J. Kimerling, 2003, Geodesic discrete global grid systems: Cartography and Geographic Information Science, **30**, 121–134, doi: 10.1559/152304003100011090.

Sava, P. C., and S. Fomel, 2003, Angle-domain common-image gathers by wavefield continuation methods: Geophysics, **68**, 1065–1074, doi: 10.1190/1.1581078.

Xie, X.-B., Z. Ge, and T. Lay, 2005, Investigating explosion source energy partitioning and Lg-wave excitation using a finite-difference plus slowness analysis method: Bulletin of the Seismological Society of America, **95**, 2412–2427, doi: 10.1785/0120050023.

Xie, X.-B., and H. Yang, 2008, A full-wave equation based seismic illumination analysis method: 70th Annual International Conference and Exhibition, EAGE, Extended Abstracts, 284.

Yan, R., and X.-B. Xie, 2012a, An angle-domain imaging condition for elastic reverse time migration and its application to angle gather extraction: Geophysics, **77**, no. 5, S105–S115, doi: 10.1190/geo2011-0455.1.

Yan, R., and X.-B. Xie, 2012b, AVA analysis based on RTM angle-domain common image gather: 82nd Annual International Meeting, SEG, Expanded Abstracts, 1–6.

Yang, H., X. Xie, M. Luo, and S. Jin, 2008, Target oriented full-wave equation based illumination analysis: 78th Annual International Meeting, SEG, Expanded Abstracts, 2216–2220.

Yilmaz, O., 2001, Seismic data analysis: SEG.

Yoon, K., and K. Marfurt, 2006, Reverse-time migration using the Poynting vector: Exploration Geophysics, **37**, 102–107, doi: 10.1071/EG06102.